

Study of $B \rightarrow K_0^*(1430) \ell^+ \ell^-$ Decay in the Standard Model and Scalar Leptoquark Scenario

M. Dadashzadeh¹ and K. Azizi^{1,2*}

¹*Department of Physics, University of Tehran, North Kargar Avenue, Tehran 14395-547, Iran*

²*Department of Physics, Dogus University, Dudullu-Ümraniye, 34775 Istanbul, Türkiye*

(Dated: February 9, 2026)

This study examines the rare decay $B \rightarrow K_0^*(1430) \ell^+ \ell^-$ as a possible probe for new physics beyond the standard model (SM). We first analyze this channel within the SM and then include scalar leptoquark (LQ) contributions. We provide predictions for key observables, like differential decay rate, branching ratio, ratio of branching fractions at different channels, forward-backward asymmetry and different lepton polarizations, and assess their sensitivity to leptoquark scenarios, highlighting q^2 regions less affected by the long-distance charmonium effects. The results can be useful for future Belle II and LHCb measurements.

I. INTRODUCTION

SM of particle physics provides a remarkably successful description of elementary particles and their interactions over a wide range of energies. Its predictive power has been confirmed in numerous colliders and low-energy experiments, resulting in the discovery of the Higgs boson in 2012. Nevertheless, the SM is widely considered to be an effective low-energy theory rather than a fundamental framework. It overlooks for the existence of dark matter and dark energy, the origin of the baryon asymmetry, neutrino oscillations, and a unified description of quark and lepton flavours. These theoretical and experimental shortcomings strongly motivate the search for new physics (NP) beyond the SM. For general reviews of flavour physics and rare B decays, see, e.g., Refs. [1–3].

Rare flavour-changing neutral current (FCNC) decays, in particular those mediated by the quark-level transition $b \rightarrow s\ell^+\ell^-$, are among the most sensitive probes of NP. In the SM, such processes arise only at the loop level through penguin and box diagrams, and their short-distance contributions are suppressed by the Glashow-Iliopoulos-Maiani (GIM) mechanism [4–6]. Consequently, the corresponding branching ratios are small, and these decays are highly sensitive to contributions from heavy virtual particles. Theoretical descriptions are formulated in terms of the weak effective Hamiltonian, where high-scale electroweak and possible NP dynamics are encoded in Wilson coefficients $C_i(\mu)$, and operator mixing is governed by renormalization-group evolution [7–9]. See also a early phenomenological analysis in Ref. [10].

Over the past decade, measurements of semileptonic B decays have revealed discrepancies from SM predictions. The LHCb Collaboration has reported persistent deviations in angular observables of the decay $B \rightarrow K^*(892)\mu^+\mu^-$, most prominently in the optimized observable P_5' [11–13], which have been tested with larger datasets and also by other experiments [14–17]. Global analyses of branching ratios and angular distributions reinforce these anomalies and suggest NP contributions predominantly in the semileptonic Wilson coefficient C_9 (and possibly C_{10}) [18–21].

Even more compelling are tests of lepton-flavour universality (LFU) in FCNC decays. Ratios such as

$$R_{K^{(*)}} = \frac{\mathcal{B}(B \rightarrow K^{(*)}\mu^+\mu^-)}{\mathcal{B}(B \rightarrow K^{(*)}e^+e^-)}, \quad (1)$$

are theoretically very clean in the SM and are predicted to be extremely close to unity, up to small electromagnetic corrections. However LHCb measurements of R_K and R_{K^*} have exhibited deviations at the level of $2\text{--}3\sigma$ [22–24], generating considerable theoretical interest. More recent LHCb and CMS analyses based on larger datasets and improved systematics have reduced some of these tensions [25, 26], yet global fits to the full set of $b \rightarrow s\ell^+\ell^-$ data still favour NP scenarios that modify the vector-current Wilson coefficients, especially C_9 , in a lepton-flavour non-universal way [27–29].

* kazem.azizi@ut.ac.ir; Corresponding author

Independent evidence for possible NP in the lepton sector arises from the long-standing discrepancy between the measured and SM-predicted values of the muon anomalous magnetic moment $a_\mu = (g_\mu - 2)/2$. The Fermilab Muon $g-2$ experiment has validated and refined the earlier Brookhaven result [30, 31], thereby increasing the tension with the state-of-the-art SM prediction based on high-precision hadronic inputs. The muon $g-2$ anomaly, together with the hints of LFU violation in B decays, motivates NP scenarios that couple non-universally to leptons and can simultaneously affect low-energy flavour observables and high-precision magnetic moment measurements.

For $b \rightarrow s\ell^+\ell^-$ transitions, an additional challenge is the control of long-distance hadronic effects, in particular those induced by intermediate charmonium resonances such as J/ψ and ψ' which strongly distort the dilepton invariant-mass spectrum when $q^2 \approx m_{cc}^2$. These contributions are encoded in the charm-loop piece of the effective coefficient C_9^{eff} and have been extensively studied using QCD factorization, light-cone sum rules and dispersion relations (e.g. [32–35]). To reduce the associated theoretical uncertainties, phenomenological analyses often focus on short-distance q^2 windows that exclude the narrow charmonium peaks.

Most experimental and theoretical work to date has concentrated on pseudoscalar and vector final states such as $B \rightarrow K\ell^+\ell^-$ and $B \rightarrow K^*(892)\ell^+\ell^-$. By contrast, scalar final states like $K_0^*(1430)$ have received comparatively less attention, despite its complementary sensitivity to the effective Hamiltonian's chiral structure. The decay $B \rightarrow K_0^*(1430)\ell^+\ell^-$ proceeds via the same underlying $b \rightarrow s\ell^+\ell^-$ transition but probes a different set of hadronic form factors and operator structures. In particular, scalar final states lead to a simpler angular distribution and can enhance the impact of scalar and pseudoscalar operators that are either absent or helicity suppressed in vector modes (see, e.g., [36–38]). This makes $B \rightarrow K_0^*(1430)\ell^+\ell^-$ an especially promising channel to explore NP with scalar interactions and non-standard chiral couplings.

Within the broad classes of NP models proposed to explain the flavour anomalies, leptoquarks (LQs) are particularly attractive. These hypothetical bosons carry both lepton and baryon quantum numbers and appear naturally in a variety of ultraviolet completions such as Pati-Salam unification, grand unified theories and models with composite fermions. They induce tree-level contributions to semileptonic four-fermion operators and are systematically classified according to their representations under $SU(3)_C \times SU(2)_L \times U(1)_Y$ [39]. Only a subset of the ten possible scalar LQ multiplets is compatible with baryon-number conservation at the renormalizable level. In the context of $b \rightarrow s\ell^+\ell^-$ anomalies, particular attention has been paid to the two $SU(2)_L$ doublets

$$X_{7/6} \equiv (3, 2, 7/6), \quad X_{1/6} \equiv (3, 2, 1/6),$$

which generate shifts in C_9 , C_{10} and their chirality-flipped counterparts and can naturally produce LFU-violating patterns in B -meson decays while remaining compatible with collider searches and other flavour constraints (see, e.g., [40–45]).

The study of $B \rightarrow K_0^*(1430)\ell^+\ell^-$ therefore offers a sensitive and complementary probe of the chiral and scalar structure of the $b \rightarrow s\ell^+\ell^-$ effective Hamiltonian. In the SM, the forward-backward asymmetry in this decay vanishes identically because of the absence of scalar couplings in the lepton sector [36]; any nonzero measurement would thus constitute a clean signal of NP. In addition, lepton-polarization observables and LFU ratios in this channel probe in detail the pattern of LQ-induced modifications to semileptonic operators and provide information that is orthogonal to that from $B \rightarrow K^{(*)}\ell^+\ell^-$.

In this study we present a detailed analysis of the decay $B \rightarrow K_0^*(1430)\ell^+\ell^-$ for $\ell = e, \mu, \tau$ within the SM and in a scalar leptoquark scenario. We employ QCD sum-rule form factors for the $B \rightarrow K_0^*(1430)$ transition [46] and implement both the short-distance SM and NP contributions using the full effective Hamiltonian including chirality-flipped operators. We compute differential decay rates, branching fractions, LFU ratios, forward-backward asymmetries and lepton-polarization asymmetries, paying particular attention to short-distance q^2 regions where long-distance charmonium effects are minimized. Our numerical analysis shows that realistic scalar LQ benchmarks can induce non-negligible and potentially observable deviations from SM expectations in several of these observables. This highlights $B \rightarrow K_0^*(1430)\ell^+\ell^-$ as a promising mode for future precision studies at Belle II and the upgraded LHCb experiment, where the non-resonant dilepton mass regions considered here will be experimentally accessible with high statistics [47–50].

Before proceeding, we briefly outline the structure of the paper. In Sec. II, we review the effective Hamiltonian for the $b \rightarrow s\ell^+\ell^-$ transition in the SM and show how it is modified in the scalar-leptoquark scenario, including the chirality-flipped operators. In Sec. III, we introduce the $B \rightarrow K_0^*(1430)$ form factors and build the decay amplitude in terms of the form factors and Wilson coefficients. In Sec. IV, we present the differential decay rate and illustrate the q^2 spectra for $\ell = e, \mu, \tau$ in the SM and with leptoquark contributions.

In Sec. V, we give numerical results for the branching fractions integrated over short-distance q^2 windows away from the J/ψ and ψ' resonances, and we discuss the LFU ratio $R_{K_0^*}$. In Sec. VI, we analyze angular and polarization observables, emphasizing the forward-backward asymmetry as a clean SM null test and showing the impact of leptoquarks on the longitudinal lepton polarization. Our conclusions are collected in Sec. VII.

II. EFFECTIVE HAMILTONIAN

Rare $b \rightarrow s\ell^+\ell^-$ transitions are most conveniently described within the framework of an effective field theory obtained after integrating out the heavy degrees of freedom (top quark, W^\pm , Z , and any heavy NP states). At scales $\mu \sim m_b$ the resulting effective weak Hamiltonian can be written as

$$\mathcal{H}_{\text{eff}} = -4 \frac{G_F}{\sqrt{2}} V_{ts}^* V_{tb} \sum_{i=1}^{10} C_i(\mu) O_i(\mu). \quad (2)$$

Here G_F is the Fermi constant, $V_{ts}^* V_{tb}$ denotes the relevant combination of CKM matrix elements, $C_i(\mu)$ are the Wilson coefficients, and $O_i(\mu)$ are local operators built from quark and lepton fields. The Wilson coefficients encode the short-distance physics and are evaluated in a given renormalization scheme (typically naive Dimensional Regularization, NDR) and evolved from the electroweak scale down to $\mu \sim m_b$ by renormalization-group methods [5, 6].

Although the full basis contains current-current, QCD penguin, electroweak penguin, and semileptonic operators, the dominant short-distance contributions to $b \rightarrow s\ell^+\ell^-$ observables arise from the magnetic dipole and semileptonic operators O_7 , O_9 , and O_{10} . The four-quark operators O_{1-6} enter indirectly through operator mixing and via long-distance $c\bar{c}$ contributions to the semileptonic amplitude. Explicitly,

$$O_7 = \frac{e}{16\pi^2} m_b (\bar{s}_\alpha \sigma^{\mu\nu} R b_\alpha) F_{\mu\nu}, \quad (3)$$

$$O_9 = \frac{e^2}{16\pi^2} (\bar{s}_\alpha \gamma^\mu L b_\alpha) (\bar{\ell} \gamma_\mu \ell), \quad (4)$$

$$O_{10} = \frac{e^2}{16\pi^2} (\bar{s}_\alpha \gamma^\mu L b_\alpha) (\bar{\ell} \gamma_\mu \gamma_5 \ell), \quad (5)$$

where $L = (1 - \gamma_5)/2$ and $R = (1 + \gamma_5)/2$ denote the left and right-handed chirality projectors. The operator O_7 drives radiative decays such as $B \rightarrow K^* \gamma$ and contributes to $B \rightarrow K^{(*)} \ell^+ \ell^-$ through a virtual photon, while $O_{9,10}$ represent vector and axial-vector semileptonic interactions.

In terms of these operators, the effective Hamiltonian relevant for $b \rightarrow s\ell^+\ell^-$ can be written as

$$\mathcal{H}_{\text{eff}} = \frac{G_F \alpha_{\text{em}} V_{tb} V_{ts}^*}{2\sqrt{2}\pi} \left[C_9^{\text{eff}}(m_b) \bar{s} \gamma_\mu (1 - \gamma_5) b \bar{\ell} \gamma^\mu \ell + C_{10}(m_b) \bar{s} \gamma_\mu (1 - \gamma_5) b \bar{\ell} \gamma^\mu \gamma_5 \ell - \frac{2m_b}{q^2} C_7^{\text{eff}}(m_b) \bar{s} i\sigma_{\mu\nu} q^\nu (1 + \gamma_5) b \bar{\ell} \gamma^\mu \ell \right]. \quad (6)$$

The coefficient C_9^{eff} contains both a perturbative short-distance part and long-distance contributions from $c\bar{c}$ intermediate states. These long-distance effects enter through the matrix elements of four-quark operators $\langle \ell^+ \ell^- s | \mathcal{O}_i | b \rangle$ with $1 \leq i \leq 6$ and can be absorbed into an effective coefficient

$$C_9^{\text{eff}}(\hat{s}) = C_9 + Y(\hat{s}), \quad \hat{s} \equiv \frac{q^2}{m_B^2}. \quad (7)$$

The Wilson coefficient C_9 is defined at the electroweak scale and evolved down to $\mu \sim m_b$ via the renormalization group, while the function $Y(\hat{s})$ encodes the effect of four-quark operators when they couple to a virtual photon subsequently producing the lepton pair [51]. The perturbative part of $Y(\hat{s})$ is a calculable loop function with GIM suppression, whereas the long-distance part associated with narrow charmonium resonances dominates in the vicinity of $q^2 \simeq m_{J/\psi}^2$ and $m_{\psi'}^2$, and cannot be reliably described by fixed-order perturbation theory [52]. In practice, one often augments the perturbative charm-loop contribution by

phenomenological Breit-Wigner terms; here, however, we focus on the short-distance regions and explicitly exclude the narrow-resonance windows.

Beyond the SM, new heavy states can generate additional operators or modify the Wilson coefficients of the existing ones. In particular, scalar leptoquarks can induce chirality-flipped operators $O'_{7,9,10}$ with opposite quark chiralities. A convenient generalized Hamiltonian including these structures is

$$\begin{aligned} \mathcal{H}_{\text{eff}} = & \frac{G_F \alpha_{\text{em}} V_{tb} V_{ts}^*}{2\sqrt{2}\pi} \left[C_9^{\text{eff}} \bar{s} \gamma_\mu (1 - \gamma_5) b \bar{\ell} \gamma^\mu \ell + C_9'^{\text{eff}} \bar{s} \gamma_\mu (1 + \gamma_5) b \bar{\ell} \gamma^\mu \ell \right. \\ & + C_{10} \bar{s} \gamma_\mu (1 - \gamma_5) b \bar{\ell} \gamma^\mu \gamma_5 \ell + C_{10}' \bar{s} \gamma_\mu (1 + \gamma_5) b \bar{\ell} \gamma^\mu \gamma_5 \ell \\ & \left. - \frac{2m_b}{q^2} C_7^{\text{eff}} \bar{s} i\sigma_{\mu\nu} q^\nu (1 + \gamma_5) b \bar{\ell} \gamma^\mu \ell - \frac{2m_b}{q^2} C_7'^{\text{eff}} \bar{s} i\sigma_{\mu\nu} q^\nu (1 - \gamma_5) b \bar{\ell} \gamma^\mu \ell \right]. \end{aligned} \quad (8)$$

In the SM, the primed coefficients are highly suppressed and can be neglected to an excellent approximation. NP can, however, introduce these chirality-flipped operators together with their associated Wilson coefficients.

In the scalar LQ model under consideration, the Wilson coefficients are modified as [41, 53]:

$$C_9^{\text{LQ}} = C_{10}^{\text{LQ}} = -\frac{\pi}{2\sqrt{2} G_F \alpha_{\text{em}} V_{tb} V_{ts}^*} \frac{\lambda_e^{23} \lambda_e^{22*}}{M_Y^2}, \quad (9)$$

$$C_9'^{\text{LQ}} = -C_{10}'^{\text{LQ}} = \frac{\pi}{2\sqrt{2} G_F \alpha_{\text{em}} V_{tb} V_{ts}^*} \frac{\lambda_s^{22} \lambda_b^{32*}}{M_V^2}. \quad (10)$$

Here $\lambda_{e,s,b}^{ij}$ denote the relevant LQ Yukawa couplings and $M_{Y,V}$ their masses. The total effective coefficients appearing in the decay amplitude then read

$$C_9^{\text{eff,tot}} = C_9^{\text{eff}} + C_9^{\text{LQ}}, \quad C_{10}^{\text{tot}} = C_{10} + C_{10}^{\text{LQ}}, \quad (11)$$

$$C_9'^{\text{eff,tot}} = C_9'^{\text{eff}} + C_9'^{\text{LQ}}, \quad C_{10}'^{\text{tot}} = C_{10}' + C_{10}'^{\text{LQ}}. \quad (12)$$

For illustration, we quote representative benchmark ranges used later:

$$C_7^{\text{eff}} = -0.295, \quad (13)$$

$$C_9^{\text{eff}} \in [1.573, 6.625], \quad (14)$$

$$C_{10} = -4.260, \quad (15)$$

$$C_9^{\text{eff,tot}} \in [2.793, 4.394], \quad (16)$$

$$C_9'^{\text{eff,tot}} \in [0, 1.586], \quad (17)$$

$$C_{10}^{\text{tot}} \in [-5.846, -4.260], \quad (18)$$

$$C_{10}'^{\text{tot}} \in [-1.586, 0], \quad (19)$$

where $C_{9,10}^{\text{LQ}}$ receive contributions from $X^{(7/6)} = (3, 2, 7/6)$ and the primed coefficients from $X^{(1/6)} = (3, 2, 1/6)$. Exact values depend on the LQ couplings and masses; here they represent benchmark intervals consistent with current constraints.

III. FORM FACTORS AND DECAY AMPLITUDE

The hadronic dynamics in the exclusive decay $B \rightarrow K_0^*(1430) \ell^+ \ell^-$ is encoded in $B \rightarrow K_0^*(1430)$ transition form factors, defined through the matrix elements

$$\langle K_0^*(1430)(p') | \bar{s} \gamma_\mu \gamma_5 b | B(p) \rangle = f_+(q^2) \mathcal{P}_\mu + f_-(q^2) q_\mu, \quad (20)$$

$$\langle K_0^*(1430)(p') | \bar{s} i\sigma_{\mu\nu} q^\nu \gamma_5 b | B(p) \rangle = \frac{f_T(q^2)}{m_B + m_{K_0^*}} \left[\mathcal{P}_\mu q^2 - (m_B^2 - m_{K_0^*}^2) q_\mu \right], \quad (21)$$

with $\mathcal{P}_\mu = (p + p')_\mu$ and $q_\mu = (p - p')_\mu$. These form factors are nonperturbative inputs and, in this work, we take them from QCD sum-rule calculations based on three-point correlation functions [46].

Concretely, one considers the correlators

$$\Pi_\mu(p, p', q) = i^2 \int d^4x d^4y e^{ip' \cdot y - ip \cdot x} \langle 0 | T \left[J^{K_0^*}(y) J_\mu^A(0) J_5^B(x) \right] | 0 \rangle, \quad (22)$$

and

$$\Pi_{\mu\nu}(p, p', q) = i^2 \int d^4x d^4y e^{ip' \cdot y - ip \cdot x} \langle 0 | T \left[J^{K_0^*}(y) J_{\mu\nu}(0) J_5^B(x) \right] | 0 \rangle, \quad (23)$$

where $J^{K_0^*} = \bar{d} s$ and $J_5^B = \bar{b} i\gamma_5 d$ are interpolating currents for $K_0^*(1430)$ and B , while $J_\mu^A = \bar{s} \gamma_\mu \gamma_5 b$ and $J_{\mu\nu} = \bar{s} i\sigma_{\mu\nu} b$ denote the transition currents. Matching the hadronic representation of these correlators to their operator-product expansion (OPE) and applying a double Borel transformation in p^2 and p'^2 yields sum rules for $f_+(q^2)$, $f_-(q^2)$, and $f_T(q^2)$. Finally, combining the matrix elements in Eqs. (20) and (21) with the generalized effective Hamiltonian (8), the $B \rightarrow K_0^*(1430) \ell^+ \ell^-$ decay amplitude can be written directly in terms of the form factors and the short-distance Wilson coefficients. It is then convenient to reorganize the result into a helicity-decomposed form,

$$\mathcal{M}(B \rightarrow K_0^* \ell^+ \ell^-) = \frac{G_F \alpha_{\text{em}}}{2\sqrt{2}\pi} V_{tb} V_{ts}^* \left\{ \bar{\ell} \gamma^\mu \ell [X_V(p + p')_\mu + Y_V q_\mu] + \bar{\ell} \gamma^\mu \gamma_5 \ell [X_A(p + p')_\mu + Y_A q_\mu] \right\}, \quad (24)$$

with the invariant amplitudes

$$X_V = (C_9^{\text{eff}} - C_9^{\text{eff}}) f_+(q^2) - \frac{2m_b}{m_B + m_{K_0^*}} (C_7^{\text{eff}} - C_7^{\text{eff}}) f_T(q^2), \quad (25)$$

$$Y_V = (C_9^{\text{eff}} - C_9^{\text{eff}}) f_-(q^2) + \frac{2m_b}{m_B + m_{K_0^*}} (C_7^{\text{eff}} - C_7^{\text{eff}}) \frac{m_B^2 - m_{K_0^*}^2}{q^2} f_T(q^2), \quad (26)$$

$$X_A = (C_{10}' - C_{10}) f_+(q^2), \quad (27)$$

$$Y_A = (C_{10}' - C_{10}) f_-(q^2). \quad (28)$$

In the SM scenario one has C_9^{eff} , C_{10} , C_7^{eff} and vanishing chirality-flipped coefficients $C_7^{\text{eff}} = C_9^{\text{eff}} = C_{10}' = 0$. In contrast, in the NP scenario considered here we use $C_9^{\text{eff}} \rightarrow C_9^{\text{eff,tot}}$, $C_9^{\text{eff}} \rightarrow C_9^{\text{eff,tot}}$, $C_{10} \rightarrow C_{10}^{\text{tot}}$, $C_{10}' \rightarrow C_{10}^{\text{tot}}$, while $C_7^{\text{eff}} = C_7^{\text{eff,tot}}$ ($C_7^{\text{eff}} = 0$), remain the same as defined in the effective Hamiltonian.

IV. DIFFERENTIAL DECAY RATE

The decay rate and angular observables are obtained from the squared matrix element, summed over final-state spins. It is convenient to express the result in terms of dimensionless kinematic variables,

$$\hat{s} = \frac{q^2}{m_B^2}, \quad \hat{m}_\ell = \frac{m_\ell}{m_B}, \quad \hat{m}_{K_0^*} = \frac{m_{K_0^*}}{m_B}, \quad (29)$$

and the Källén function

$$\lambda(\hat{s}) = 1 + \hat{m}_{K_0^*}^4 + \hat{s}^2 - 2\hat{s} - 2\hat{m}_{K_0^*}^2(1 + \hat{s}), \quad (30)$$

and

$$v = \sqrt{1 - \frac{4\hat{m}_\ell^2}{\hat{s}}}. \quad (31)$$

The variable v represents the velocity of the lepton in the dilepton rest frame.

After integrating over the lepton polar angle, the single differential rate for $B \rightarrow K_0^*(1430) \ell^+ \ell^-$ can be written as

$$\frac{d\Gamma}{d\hat{s}} = \frac{G_F^2 \alpha_{\text{em}}^2 |V_{tb} V_{ts}^*|^2}{2048\pi^5} m_B^5 \sqrt{\lambda(\hat{s})} v \left[\frac{\lambda(\hat{s}) v^2}{3} \left(|X_V|^2 + |X_A|^2 \right) + \frac{\hat{m}_\ell^2}{\hat{s}} \left(|X_V(1 - \hat{m}_{K_0^*}^2) + Y_V \hat{s}|^2 + |X_A(1 - \hat{m}_{K_0^*}^2) + Y_A \hat{s}|^2 \right) \right]. \quad (32)$$

The first term, proportional to $\lambda(\hat{s}) v^2/3$, dominates for light leptons ($\ell = e, \mu$) and encodes the contributions from transverse helicity configurations. The second term, proportional to \hat{m}_ℓ^2/\hat{s} , becomes relevant for heavier leptons (e.g. τ) and probes combinations of the scalar kinematic structures Y_V and Y_A . In particular, this term can be enhanced in scenarios with large scalar or pseudoscalar contributions, although such operators are absent in the SM for light leptons.

V. NUMERICAL RESULTS

A. Differential decay-rate spectra

Numerically, we use the $B \rightarrow K_0^*(1430)$ form factors from Ref. [46] together with the Wilson coefficients specified in Sec. II. The resulting differential spectra $d\Gamma/d\hat{s}$ with $\hat{s} \equiv q^2/m_B^2$ are shown in Figs. 1a–1c for $\ell = e, \mu, \tau$, comparing the SM with representative scalar-leptoquark (LQ) benchmarks. In each panel, the blue shaded band represents the SM prediction and the pink band the LQ scenario; the purple region corresponds to the overlap of the two semi-transparent bands. The band widths reflect the combined theoretical uncertainty from the form factors and from varying the Wilson coefficients within the benchmark ranges of Sec. II.

For $\ell = e, \mu$, the spectra are largest at low q^2 and decrease towards the endpoint $q_{\text{max}}^2 = (m_B - m_{K_0^*})^2$, as expected from the shrinking phase space at large dilepton invariant mass. The enhancement at low q^2 is driven by the photon-penguin contribution associated with C_7^{eff} , which is amplified by the $1/q^2$ factor in the amplitude. At low and intermediate q^2 , the semileptonic operators proportional to C_9^{eff} and C_{10} give additional contributions and interference terms that shape the spectra. For the scalar-LQ benchmarks considered here, the predicted rates are typically reduced with respect to the SM over most of the accessible range (pink band below blue), with the largest relative effect in the region where the interplay of C_7^{eff} and C_9^{eff} is most pronounced.

In the $\tau^+ \tau^-$ channel, the spectrum starts only at the physical threshold $q^2 \geq 4m_\tau^2$, so only the high- q^2 region is accessible (Fig. 1c). In this regime the photon-penguin term is comparatively less important, and the rate is dominated by the semileptonic contributions controlled by C_9^{eff} and C_{10} , modulated by the reduced available phase space. Consequently, the SM and LQ predictions differ mainly through an overall normalization, while the shape of the spectrum is less strongly modified than in the light-lepton modes.

The overall shape of the spectra is largely governed by phase space and the helicity structure of the $b \rightarrow s \ell^+ \ell^-$ transition. For $\ell = e, \mu$, the rate is largest at low q^2 and decreases towards the kinematic endpoint $q_{\text{max}}^2 = (m_B - m_{K_0^*})^2$, reflecting the shrinking phase space at large dilepton invariant mass. At low and intermediate q^2 the decay is mainly driven by the vector contribution proportional to C_9^{eff} together with the photon-penguin term governed by C_7^{eff} , while the axial-vector piece proportional to C_{10} enters through $|C_{10}|^2$ and through interference with the vector amplitude. The scalar-LQ benchmarks considered here modify these short-distance coefficients, leading predominantly to a suppression of the rate relative to the SM (red band below blue) over most of the accessible range. The effect is most visible where the $C_9^{\text{eff}} - C_7^{\text{eff}}$ interplay and their interference with C_{10} provide the dominant contribution, i.e. away from the endpoint.

For $\ell = \tau$, the spectrum starts only at threshold $q^2 \geq 4m_\tau^2$ and is therefore confined to the high- q^2 region shown in Fig. 1c. In this regime the photon-penguin contribution is less important, and the rate is more strongly shaped by the semileptonic operators governed by C_9^{eff} and C_{10} together with the reduced available phase space. As a consequence, the SM and LQ predictions differ mainly through an overall normalization, while the spectral shape is less dramatically distorted, consistent with the limited kinematic lever arm in the $\tau^+ \tau^-$ channel.

Overall, as is seen, the differential decay rate for the LQ and SM scenarios show large overlap regions for all leptons. For $\ell = e, \mu$, LQ scans some narrow regions out of the SM bands.

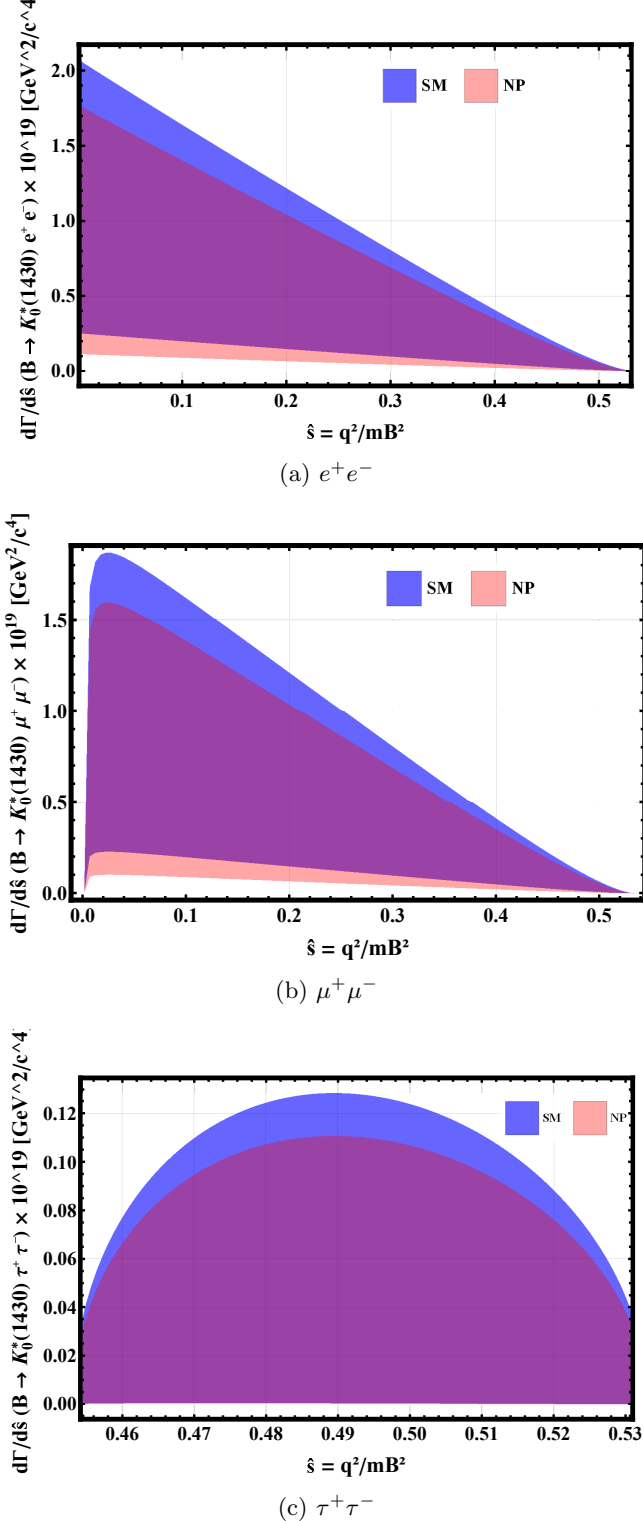


FIG. 1: Differential decay rate for $B \rightarrow K_0^*(1430) \ell^+ \ell^-$ in the SM and in the scalar LQ scenario ($\ell = e, \mu, \tau$). For $\tau^+ \tau^-$ the spectrum starts at $q^2 \geq 4m_\tau^2$, so the low- q^2 region is not accessible.

B. Other observables results

Having established the differential spectra, we now turn to integrated observables that are directly relevant for phenomenology and comparison with experimental data. In particular, we present numerical predictions for the partially integrated branching fractions and their ratios at different lepton channels for tests of lepton-flavour universality (LFU) in $B \rightarrow K_0^*(1430)\ell^+\ell^-$, both in the SM and in the scalar-LQ scenario. These quantities probe complementary combinations of the short-distance Wilson coefficients and are less sensitive to bin-by-bin fluctuations of the spectrum.

A central issue in $b \rightarrow s\ell^+\ell^-$ phenomenology is the presence of long-distance hadronic effects associated with intermediate charmonium states, which strongly enhance the rate when $q^2 \simeq m_{J/\psi}^2$ or $m_{\psi'}^2$, and can obscure potential short-distance NP contributions. To reduce this impact, we follow a standard strategy by partition of the kinematically allowed q^2 range into three different regions, removing symmetric veto windows around the J/ψ and ψ' resonances. We then integrate the differential rate over each region to obtain partial branching fractions, and construct LFU ratios by taking appropriate muon-to-electron (and, where applicable, tau-to-muon/electron) combinations. In this way, the resulting observables retain high sensitivity to the LQ-induced shifts in the semileptonic coefficients while minimizing the dominant charmonium-related uncertainties.

The physical ranges are

$$\begin{aligned} \text{Region I: } & 4m_\ell^2 \leq q^2 \leq (m_{J/\psi} - 0.02 \text{ GeV})^2, \\ \text{Region II: } & (m_{J/\psi} + 0.02 \text{ GeV})^2 \leq q^2 \leq (m_{\psi'} - 0.02 \text{ GeV})^2, \\ \text{Region III: } & (m_{\psi'} + 0.02 \text{ GeV})^2 \leq q^2 \leq (m_B - m_{K_0^*})^2, \end{aligned}$$

with $m_{J/\psi} = 3.0969 \text{ GeV}$, $m_{\psi'} = 3.6861 \text{ GeV}$, $m_B = 5.279 \text{ GeV}$, and $m_{K_0^*} = 1.425 \text{ GeV}$. Region I corresponds to the low- q^2 domain, Region II to the intermediate- q^2 window between the two charmonium peaks, and Region III to the high- q^2 endpoint region.

The integrated branching ratios in each region, including uncertainties from the form factors and variations of the Wilson coefficients within their benchmark ranges, are collected in Tables I, II and III for the ℓ , μ and τ channels, respectively, where the large relative uncertainty in the τ channel reflects both the limited phase space and the enhanced sensitivity to helicity-suppressed contributions.

TABLE I: Branching ratios for $B \rightarrow K_0^*(1430)e^+e^-$ in the SM and in the scalar LQ model. The quoted ranges reflect combined uncertainties from form factors and Wilson coefficients.

Region	SM (Range)	LQ (Range)
Region I (Low q^2)	$[1.28 - 10.57] \times 10^{-8}$	$[0.57 - 9.04] \times 10^{-8}$
Region II (J/ψ gap)	$[0.13 - 1.08] \times 10^{-8}$	$[0.06 - 0.93] \times 10^{-8}$
Region III (High q^2)	$[0.04 - 0.31] \times 10^{-9}$	$[0.02 - 0.27] \times 10^{-9}$
Total (3 regions)	$[1.43 - 11.83] \times 10^{-8}$	$[0.64 - 10.12] \times 10^{-8}$

TABLE II: Branching ratios for $B \rightarrow K_0^*(1430)\mu^+\mu^-$ in the SM and in the scalar LQ model. The quoted ranges reflect combined uncertainties from form factors and Wilson coefficients.

Region	SM (Range)	LQ (Range)
Region I (Low q^2)	$[1.24 - 10.23] \times 10^{-8}$	$[0.55 - 8.75] \times 10^{-8}$
Region II (J/ψ gap)	$[0.13 - 1.09] \times 10^{-8}$	$[0.06 - 0.93] \times 10^{-8}$
Region III (High q^2)	$[0.04 - 0.32] \times 10^{-9}$	$[0.02 - 0.27] \times 10^{-9}$
Total (3 regions)	$[1.39 - 11.50] \times 10^{-8}$	$[0.62 - 9.84] \times 10^{-8}$

TABLE III: Branching ratios for $B \rightarrow K_0^*(1430) \tau^+ \tau^-$ in the SM and in the scalar LQ model. Region I is kinematically forbidden for $\tau^+ \tau^-$ because $q^2 < 4m_\tau^2$. The quoted ranges reflect combined uncertainties from form factors and Wilson coefficients.

Region	SM (Range)	LQ (Range)
Region I (Low q^2)	$q^2 < 4m_\tau^2$ (forbidden)	
Region II (J/ψ gap)	$[0.03 - 6.08] \times 10^{-10}$	$[0.01 - 5.24] \times 10^{-10}$
Region III (High q^2)	$[0.02 - 8.94] \times 10^{-10}$	$[0.01 - 7.71] \times 10^{-10}$
Total (physical q^2)	$[0.06 - 18.47] \times 10^{-10}$	$[0.02 - 15.92] \times 10^{-10}$

Although, large intersections between the SM and LQ models are seen, there are some narrow regions for LQ out of the SM predictions considering all the uncertainties.

To test lepton-flavour universality in $B \rightarrow K_0^*(1430) \ell^+ \ell^-$, we define

$$R_{K_0^*} \equiv \frac{\mathcal{B}(B \rightarrow K_0^*(1430) \mu^+ \mu^-)}{\mathcal{B}(B \rightarrow K_0^*(1430) e^+ e^-)}, \quad (33)$$

where the branching fractions are integrated over the same short-distance q^2 regions (with the J/ψ and ψ' vetoes) as in Tabs. I–II. Using the corresponding total integrated ranges, we obtain

$$R_{K_0^*}^{\text{SM}} \in [0.9673, 0.9721], \quad (34)$$

$$R_{K_0^*}^{\text{LQ}} \in [0.9659, 0.9723]. \quad (35)$$

As expected, $R_{K_0^*}$ is very close to unity in both scenarios. The dominant hadronic uncertainties largely cancel in the ratio, while the remaining deviation from 1 is mainly driven by lepton-mass effects and the slightly different kinematics between the e and μ modes (together with small residual differences induced by the chosen short-distance windows). For the scalar-LQ benchmarks considered here, the predicted shift in $R_{K_0^*}$ is modest, indicating no sizeable LFU violation in the μ/e sector for these parameter choices.

A complementary ratio involving τ leptons can be defined only in kinematic regions accessible to both $\mu^+ \mu^-$ and $\tau^+ \tau^-$. We therefore focus on the high- q^2 window (Region III) and define

$$R_{K_0^*}^{\tau\mu}|_{\text{III}} \equiv \frac{\mathcal{B}_{\text{III}}(B \rightarrow K_0^*(1430) \tau^+ \tau^-)}{\mathcal{B}_{\text{III}}(B \rightarrow K_0^*(1430) \mu^+ \mu^-)}, \quad (36)$$

where \mathcal{B}_{III} denotes integration over Region III only. From Tabs. II and III, we find the indicative ranges

$$R_{K_0^*}^{\tau\mu}|_{\text{III, SM}} \in [4.96 \times 10^{-3}, 2.41 \times 10^1], \quad R_{K_0^*}^{\tau\mu}|_{\text{III, LQ}} \in [2.16 \times 10^{-3}, 2.08 \times 10^1]. \quad (37)$$

The wide spread is a direct consequence of the much larger relative uncertainty in the $\tau^+ \tau^-$ mode: since $q_{\text{max}}^2 = (m_B - m_{K_0^*})^2$ lies only moderately above the threshold $4m_\tau^2$, the available phase space is compressed near the endpoint, enhancing the sensitivity to form-factor variations and to helicity-suppressed contributions. As a result, $R_{K_0^*}^{\tau\mu}$ is less constraining in a conservative range scan, but it remains a useful high- q^2 LFU probe once uncertainties are reduced and more targeted benchmark choices are adopted.

VI. FORWARD-BACKWARD ASYMMETRY AND LEPTON POLARIZATION

Angular observables provide additional, and often more reliable, probes of the underlying short-distance dynamics. In particular, the forward-backward asymmetry of the lepton and the lepton polarization asymmetries are sensitive to the chiral and scalar structure of the effective Hamiltonian and can help disentangle different NP scenarios.

The double differential decay width in the dilepton invariant mass q^2 and the angle θ between the momentum of the negatively charged lepton ℓ^- and the K_0^* in the dilepton rest frame can be written as

$$\frac{d^2\Gamma}{dq^2 d\cos\theta} = \frac{1}{512\pi^3 m_B^3} \lambda^{1/2}(m_B^2, m_{K_0^*}^2, q^2) \beta_\ell \sum_{\text{spins}} |\mathcal{M}|^2,$$

with the usual kinematic functions

$$\beta_\ell = \sqrt{1 - \frac{4m_\ell^2}{q^2}}, \quad L \equiv \frac{\beta_\ell \sqrt{\lambda}}{4}.$$

After carrying out the spin sums and expressing the result in terms of $X_{V,A}$ and $Y_{V,A}$, the angular distribution of the $B \rightarrow K_0^* \ell^+ \ell^-$ decay can be cast in the compact form

$$\frac{d^2\Gamma}{dq^2 d\cos\theta} = \mathcal{P}(q^2) [\mathcal{C}_0(q^2) + \mathcal{C}_2(q^2) \cos^2\theta], \quad (38)$$

where the common prefactor is

$$\mathcal{P}(q^2) = \frac{1}{512\pi^3 m_B^3} \lambda^{1/2}(m_B^2, m_{K_0^*}^2, q^2) \beta_\ell \cdot 4|N|^2, \quad (39)$$

and $N = \frac{G_F \alpha_{\text{em}} V_{tb} V_{ts}^*}{2\sqrt{2}\pi}$.

Defining the auxiliary combinations

$$V \cdot V = X_V^2 P^2 + 2 X_V Y_V \Delta + Y_V^2 q^2, \quad (40)$$

$$A \cdot A = X_A^2 P^2 + 2 X_A Y_A \Delta + Y_A^2 q^2, \quad (41)$$

$$P^2 = 2(m_B^2 + m_{K_0^*}^2) - q^2, \quad (42)$$

one finds

$$\mathcal{C}_0(q^2) = 2 \left[(X_V K + Y_V Q)^2 + (X_A K + Y_A Q)^2 \right] - \frac{1}{2} q^2 (V \cdot V + A \cdot A), \quad (43)$$

$$\mathcal{C}_2(q^2) = -2 L^2 (X_V^2 + X_A^2), \quad (44)$$

where K and Q are simple kinematic functions of the masses and q^2 (their explicit expressions can be found from the full decomposition of the amplitude but are not needed here).

The forward-backward asymmetry (FBA) is defined in the standard way as

$$A_{FB}(q^2) = \frac{\int_0^1 d\cos\theta \frac{d^2\Gamma(q^2, \cos\theta)}{dq^2 d\cos\theta} - \int_{-1}^0 d\cos\theta \frac{d^2\Gamma(q^2, \cos\theta)}{dq^2 d\cos\theta}}{\int_0^1 d\cos\theta \frac{d^2\Gamma(q^2, \cos\theta)}{dq^2 d\cos\theta} + \int_{-1}^0 d\cos\theta \frac{d^2\Gamma(q^2, \cos\theta)}{dq^2 d\cos\theta}}. \quad (45)$$

For a scalar final state such as $K_0^*(1430)$, and in the absence of scalar-type lepton couplings, the angular dependence reduces to an even function of $\cos\theta$. It follows that the numerator of $A_{FB}(q^2)$ vanishes identically in the SM, and $A_{FB}(q^2) = 0$ for all q^2 [36]. This makes the FBA in $B \rightarrow K_0^*(1430) \ell^+ \ell^-$ a particularly clean null test of the SM: any non-zero measurement would point directly to NP with scalar or pseudoscalar couplings.

In addition to the FBA, lepton polarization asymmetries provide complementary information on the chiral structure of the underlying short-distance dynamics. For a given spin direction $\hat{\mathbf{i}}$ ($i = L, T, N$), we define

$$P_i(q^2) = \frac{\frac{d\Gamma}{dq^2}(\hat{\mathbf{s}}_- = +\hat{\mathbf{i}}) - \frac{d\Gamma}{dq^2}(\hat{\mathbf{s}}_- = -\hat{\mathbf{i}})}{\frac{d\Gamma}{dq^2}(\hat{\mathbf{s}}_- = +\hat{\mathbf{i}}) + \frac{d\Gamma}{dq^2}(\hat{\mathbf{s}}_- = -\hat{\mathbf{i}})}, \quad (46)$$

where L, T, N denote the longitudinal, transverse, and normal polarizations of ℓ^- , respectively. We work in the dilepton rest frame, choose the z -axis along the K_0^* momentum, and define the $x-z$ plane as the decay

plane spanned by $\vec{p}_{K_0^*}$ and \vec{p}_{ℓ^-} . The spin unit vectors in the ℓ^- rest frame are taken as

$$\hat{\mathbf{s}}_L = \frac{\vec{p}_{\ell^-}}{|\vec{p}_{\ell^-}|}, \quad (47)$$

$$\hat{\mathbf{s}}_N = \frac{\vec{p}_{K_0^*} \times \vec{p}_{\ell^-}}{|\vec{p}_{K_0^*} \times \vec{p}_{\ell^-}|}, \quad (48)$$

$$\hat{\mathbf{s}}_T = \hat{\mathbf{s}}_N \times \hat{\mathbf{s}}_L. \quad (49)$$

Using the amplitude in Eq. (24) and the invariant functions X_V, Y_V, X_A, Y_A defined in Eqs. (25)–(28), the longitudinal polarization of ℓ^- in the *integrated* dilepton spectrum can be written in the compact form

$$P_L(\hat{s}) = \frac{4v \Re[X_V(\hat{s}) X_A^*(\hat{s})]}{2v^2 |X_V(\hat{s})|^2 + (3-v^2) |X_A(\hat{s})|^2}. \quad (50)$$

For the decay $B \rightarrow K_0^* \ell^+ \ell^-$ (spinless hadronic final state), the normal and transverse polarizations are canceled after angular integration, so that

$$P_N(\hat{s}) = 0, \quad P_T(\hat{s}) = 0, \quad (51)$$

and P_L is the only non-trivial single-lepton polarization observable in the integrated dilepton spectrum.

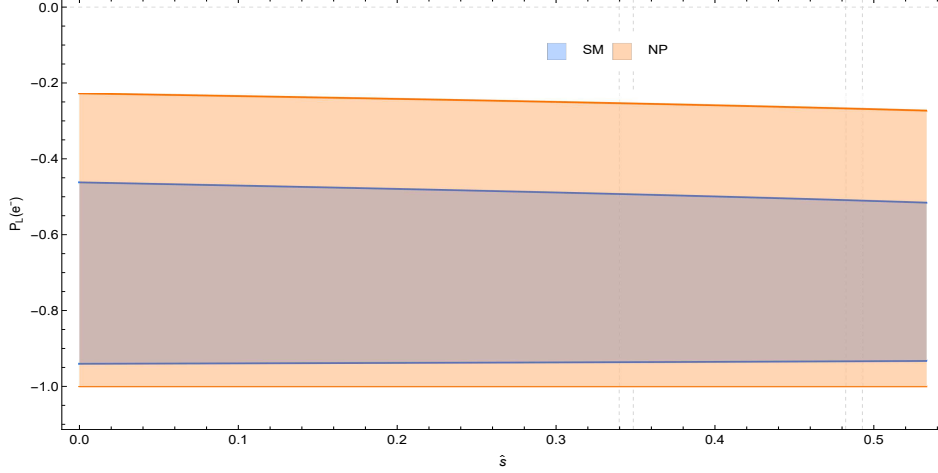
The longitudinal lepton polarization asymmetry $P_L(\hat{s})$ for the decays $B \rightarrow K_0^*(1430) \ell^+ \ell^-$ is shown in Fig. 2 as a function of the dilepton invariant mass squared q^2 for $\ell = e, \mu, \tau$. The individual panels correspond to the electron, muon, and tau channels in Figs. 2a, 2b, and 2c, respectively. In each case, the SM prediction is compared with the scalar leptoquark scenario, illustrating the sensitivity of P_L to the underlying short-distance dynamics.

Since $P_L(\hat{s})$ is defined as a ratio of polarized decay rates, it is bounded by $-1 \leq P_L(\hat{s}) \leq 1$. Negative values correspond to a predominantly left-handed ℓ^- , which is the expected pattern in the SM because the weak interaction is chiral [54].

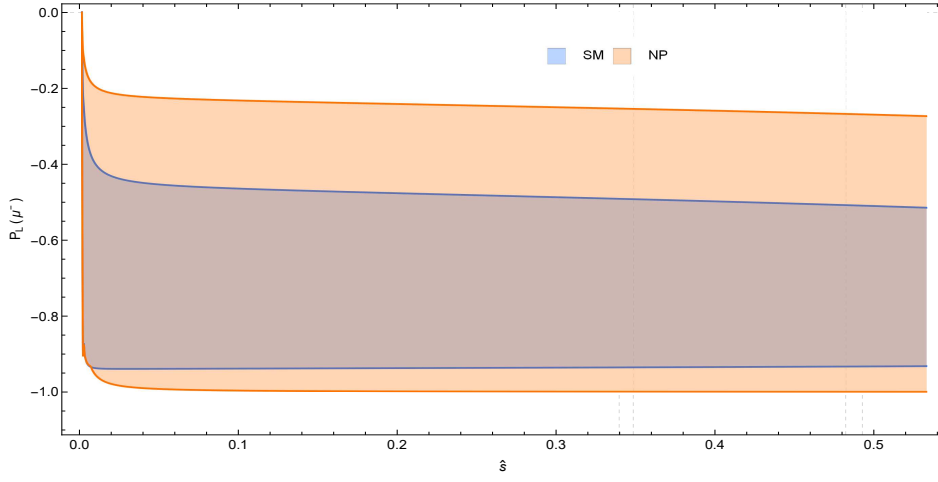
Figure 2 shows $P_L(\hat{s})$ for $B \rightarrow K_0^*(1430) \ell^+ \ell^-$ with $\ell = e, \mu, \tau$, comparing the SM prediction (blue band) to the scalar leptoquark scenario (orange band). For the light-lepton modes, $B \rightarrow K_0^*(1430) e^+ e^-$ and $B \rightarrow K_0^*(1430) \mu^+ \mu^-$ (Figs. 2a and 2b), the SM result stays close to $P_L(\hat{s}) \simeq -1$ across almost the entire kinematic range, indicating that the final-state lepton is produced nearly purely left-handed [54]. In the leptoquark case the polarization remains negative, but the magnitude is reduced, so that typically, considering the averages, $|P_L^{\text{NP}}(\hat{s})| < |P_L^{\text{SM}}(\hat{s})|$ throughout the accessible \hat{s} region. Physically, this reflects the presence of additional contributions in the NP scenario that populate the opposite-helicity component and therefore dilute the net longitudinal polarization [54].

The situation changes noticeably for the τ channel in Fig. 2c. Because m_τ is large, helicity suppression is much less effective, and the SM prediction develops a clear \hat{s} dependence, with $P_L(\hat{s})$ departing significantly from -1 towards the upper end of phase space [54]. In the scalar leptoquark scenario this effect becomes even more pronounced: scalar-type contributions scale with the lepton mass and are therefore most important for $\ell = \tau$, leading to a smaller $|P_L(\hat{s})|$. As a result, the longitudinal polarization in $B \rightarrow K_0^*(1430) \tau^+ \tau^-$ offers a particularly sensitive handle on scalar leptoquark effects in rare B decays [54].

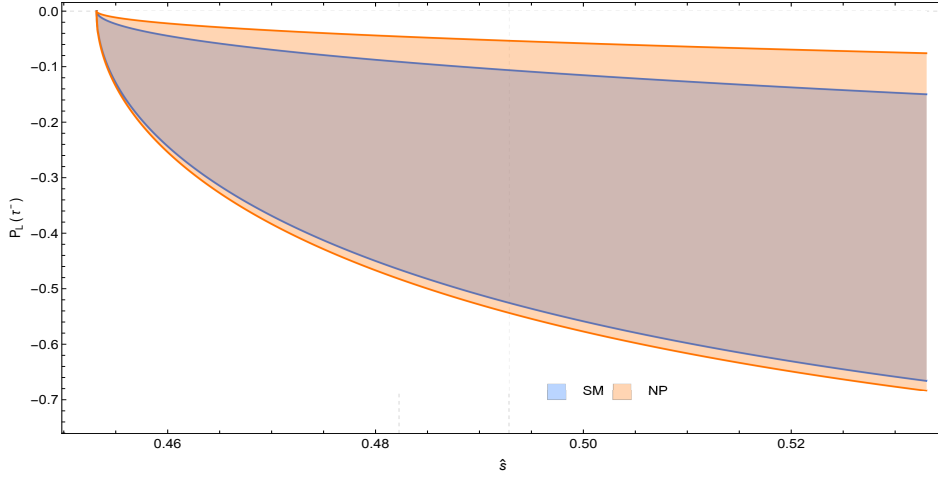
In summary, $P_L(\hat{s})$ is nearly saturated at -1 and only weakly depends on \hat{s} for $\ell = e, \mu$, while for $\ell = \tau$ both the kinematic variation and the size of possible deviations from the SM are enhanced, especially at large \hat{s} [54].



(a) Longitudinal lepton polarization asymmetry P_L for $B \rightarrow K_0^*(1430) e^+ e^-$ in the SM and the scalar leptoquark scenario.



(b) Longitudinal lepton polarization asymmetry P_L for $B \rightarrow K_0^*(1430) \mu^+ \mu^-$ in the SM and the scalar leptoquark scenario.



(c) Longitudinal lepton polarization asymmetry P_L for $B \rightarrow K_0^*(1430) \tau^+ \tau^-$ in the SM and the scalar leptoquark scenario.

FIG. 2: Longitudinal lepton polarization asymmetry $P_L(\hat{s})$ in $B \rightarrow K_0^*(1430) \ell^+ \ell^-$ for $\ell = e, \mu, \tau$, comparing the SM prediction with the scalar leptoquark scenario.

VII. CONCLUSIONS

In this work, we studied the rare decay $B \rightarrow K_0^*(1430)\ell^+\ell^-$ with $\ell = e, \mu, \tau$ as a sensitive probe of new physics in $b \rightarrow s\ell^+\ell^-$ transitions, focusing on scalar leptoquark scenarios that can accommodate current flavour anomalies and the muon anomalous magnetic moment. On the SM side, we expressed the semileptonic amplitude in terms of the usual effective coefficients and concentrated on short-distance q^2 windows. By imposing explicit vetoes around the J/ψ and ψ' resonances, we strongly suppressed long-distance charmonium effects and kept theoretical uncertainties under control. Using QCD sum-rule form factors for the $B \rightarrow K_0^*(1430)$ transition, we derived analytic expressions and presented numerical predictions for the differential decay rate, partially integrated branching fractions, LFU ratios, and lepton polarization observables in these clean kinematic regions.

We then analyzed the same observables in a scalar-leptoquark framework in which tree level semileptonic interactions induce shifts in C_9, C_{10} and their chirality-flipped counterparts. In this setup we find sizeable, but still experimentally realistic, departures from SM expectations. For the light lepton modes, the branching fractions integrated over the three short-distance regions fall in the ranges $\mathcal{B}(B \rightarrow K_0^*(1430)e^+e^-)_{\text{SM}} \simeq (1.4-11.8) \times 10^{-8}$ and $\mathcal{B}(B \rightarrow K_0^*(1430)\mu^+\mu^-)_{\text{SM}} \simeq (1.4-11.5) \times 10^{-8}$, while the scalar leptoquark benchmarks typically lower them to about $(0.6-10.1) \times 10^{-8}$ and $(0.6-9.8) \times 10^{-8}$, respectively. In other words, within the quoted uncertainties, the new physics benchmarks can suppress the average rates by up to $\mathcal{O}(20\%)$ across the short-distance regions. The τ mode is much rarer, $\mathcal{B}(B \rightarrow K_0^*(1430)\tau^+\tau^-) \sim (0.6-1.8) \times 10^{-9}$ in the SM and $(0.2-1.6) \times 10^{-9}$ in the leptoquark scenario, but it remains particularly informative because helicity-suppressed effects are less severe and the decay is therefore more sensitive to the chiral structure of possible new interactions.

Lepton flavour universality tests constructed from the electron and muon channels, and especially

$$R_{K_0^*} \equiv \frac{\mathcal{B}(B \rightarrow K_0^*(1430)\mu^+\mu^-)}{\mathcal{B}(B \rightarrow K_0^*(1430)e^+e^-)},$$

stay extremely close to unity in both scenarios: $R_{K_0^*}^{\text{SM}} \in [0.9673, 0.9721]$ and $R_{K_0^*}^{\text{LQ}} \in [0.9659, 0.9723]$. This behaviour is expected: hadronic uncertainties largely cancel in the ratio and lepton mass effects are tiny in the μ/e sector. As a result, the benchmark leptoquark couplings considered here do not predict large LFU violation between electrons and muons in this channel. Ratios involving τ leptons, such as $R_{K_0^*}^{\tau\mu}$ in the high q^2 region, span a wider range because the available phase space is strongly compressed near threshold. Nevertheless, with improved form factor input and more targeted benchmark choices, these observables could become useful probes of non-universality at high q^2 .

Angular and polarization observables provide an especially clean handle on short-distance dynamics in this decay. Since the hadronic final state is a scalar and the SM does not contain scalar lepton couplings, the forward-backward asymmetry $A_{FB}(q^2)$ vanishes identically for all q^2 . Therefore, any nonzero measurement of A_{FB} in $B \rightarrow K_0^*(1430)\ell^+\ell^-$ would be a direct indication of non-standard scalar or pseudoscalar interactions. The longitudinal lepton polarization $P_L(\hat{s})$ is also very distinctive: for $\ell = e, \mu$ it is nearly maximally negative and only weakly dependent on \hat{s} in the SM, whereas scalar leptoquarks reduce $|P_L|$ by enhancing the opposite helicity component, producing a characteristic shift that is largely insensitive to hadronic input. For $\ell = \tau$, $P_L(\hat{s})$ shows a much stronger \hat{s} dependence and an even clearer separation between SM and leptoquark predictions, making the $\tau^+\tau^-$ mode a particularly sensitive probe of scalar new physics in the high- q^2 region.

To summarize, $B \rightarrow K_0^*(1430)\ell^+\ell^-$ provides a theoretically clean and phenomenologically rich complement to the better studied $B \rightarrow K^{(*)}\ell^+\ell^-$ modes. In the short-distance windows that will be accessible at Belle II and the upgraded LHCb, improved measurements of differential rates, integrated branching fractions, LFU ratios, and especially longitudinal lepton polarization can either reveal scalar leptoquark effects or place strong constraints on them, as well as on other extensions of the SM that modify the chiral or scalar structure of $b \rightarrow s\ell^+\ell^-$. On the theory side, more precise nonperturbative determinations of the $B \rightarrow K_0^*(1430)$ form factors and a refined treatment of residual long-distance effects will further sharpen these predictions and strengthen the discovery potential of this channel in the high luminosity era.

ACKNOWLEDGMENTS

K. Azizi thanks the Iran National Science Foundation (INSF) for partial financial support provided under the Elites Grant No. 40405095.

[1] T. E. Browder, T. Gershon, D. Pirjol, A. Soni and J. Zupan, Rev. Mod. Phys. **81**, 1887–1941 (2009) [doi:10.1103/RevModPhys.81.1887](https://doi.org/10.1103/RevModPhys.81.1887) arXiv:0802.3201 [hep-ph].

[2] J. D. Richman [BaBar and Belle], Nucl. Phys. Proc. Suppl. **170**, 193–198 (2007) [doi:10.1016/j.nuclphysbps.2007.05.040](https://doi.org/10.1016/j.nuclphysbps.2007.05.040).

[3] P. H. Owen, PhD Thesis, University of Warwick (2014) [doi:10.25560/24751](https://doi.org/10.25560/24751).

[4] G. Buchalla, A. J. Buras and M. E. Lautenbacher, Rev. Mod. Phys. **68**, 1125–1144 (1996) [doi:10.1103/RevModPhys.68.1125](https://doi.org/10.1103/RevModPhys.68.1125) arXiv:hep-ph/9512380.

[5] A. J. Buras, M. Misiak, M. Münz and S. Pokorski, Nucl. Phys. B **424**, 374–398 (1994) [doi:10.1016/0550-3213\(94\)90299-2](https://doi.org/10.1016/0550-3213(94)90299-2) arXiv:hep-ph/9311345.

[6] A. J. Buras and M. Münz, Phys. Rev. D **52**, 186–195 (1995) [doi:10.1103/PhysRevD.52.186](https://doi.org/10.1103/PhysRevD.52.186) arXiv:hep-ph/9501281 [hep-ph].

[7] A. J. Buras, “Weak Hamiltonian, CP violation and rare decays,” in *Probing the Standard Model of Particle Interactions*, [doi:10.48550/arXiv.hep-ph/9806471](https://doi.org/10.48550/arXiv.hep-ph/9806471) arXiv:hep-ph/9806471 [hep-ph].

[8] G. Isidori, Y. Nir and G. Perez, Ann. Rev. Nucl. Part. Sci. **60**, 355–378 (2010) [doi:10.1146/annurev.nucl.012809.104534](https://doi.org/10.1146/annurev.nucl.012809.104534) arXiv:1002.0900 [hep-ph].

[9] T. Hurth, Rev. Mod. Phys. **75**, 1159–1199 (2003) [doi:10.1103/RevModPhys.75.1159](https://doi.org/10.1103/RevModPhys.75.1159) arXiv:hep-ph/0212304 [hep-ph].

[10] A. Ali, E. Lunghi, C. Greub and G. Hiller, Phys. Rev. D **66**, 034002 (2002) [doi:10.1103/PhysRevD.66.034002](https://doi.org/10.1103/PhysRevD.66.034002) arXiv:hep-ph/0112300 [hep-ph].

[11] R. Aaij *et al.* [LHCb], Phys. Rev. Lett. **111**, 191801 (2013) [doi:10.1103/PhysRevLett.111.191801](https://doi.org/10.1103/PhysRevLett.111.191801) arXiv:1308.1707 [hep-ex].

[12] R. Aaij *et al.* [LHCb], JHEP **02**, 104 (2016) [doi:10.1007/JHEP02\(2016\)104](https://doi.org/10.1007/JHEP02(2016)104) arXiv:1512.04442 [hep-ex].

[13] C. Bobeth, G. Hiller and D. van Dyk, JHEP **07**, 067 (2011) [doi:10.1007/JHEP07\(2011\)067](https://doi.org/10.1007/JHEP07(2011)067) arXiv:1105.0376 [hep-ph].

[14] R. Aaij *et al.* [LHCb], Phys. Rev. Lett. **125**, 011802 (2020) [doi:10.1103/PhysRevLett.125.011802](https://doi.org/10.1103/PhysRevLett.125.011802) arXiv:2003.04831 [hep-ex].

[15] R. Aaij *et al.* [LHCb], Phys. Rev. D **108**, 032002 (2023) [doi:10.1103/PhysRevD.108.032002](https://doi.org/10.1103/PhysRevD.108.032002) arXiv:2212.09153 [hep-ex].

[16] A. M. Sirunyan *et al.* [CMS], Phys. Lett. B **781**, 517–541 (2018) [doi:10.1016/j.physletb.2018.04.030](https://doi.org/10.1016/j.physletb.2018.04.030) arXiv:1710.02846 [hep-ex].

[17] M. Aaboud *et al.* [ATLAS], JHEP **10**, 047 (2018) [doi:10.1007/JHEP10\(2018\)047](https://doi.org/10.1007/JHEP10(2018)047) arXiv:1805.04000 [hep-ex].

[18] W. Altmannshofer and D. M. Straub, Eur. Phys. J. C **75**, 382 (2015) [doi:10.1140/epjc/s10052-015-3602-7](https://doi.org/10.1140/epjc/s10052-015-3602-7) arXiv:1411.3161 [hep-ph].

[19] B. Capdevila, A. Crivellin, S. Descotes-Genon, J. Matias and J. Virto, JHEP **01**, 093 (2018) [doi:10.1007/JHEP01\(2018\)093](https://doi.org/10.1007/JHEP01(2018)093) arXiv:1704.05340 [hep-ph].

[20] G. Hiller and F. Krüger, Phys. Rev. D **69**, 074020 (2004) [doi:10.1103/PhysRevD.69.074020](https://doi.org/10.1103/PhysRevD.69.074020) arXiv:hep-ph/0310219 [hep-ph].

[21] S. Descotes-Genon, J. Matias and J. Virto, Phys. Rev. D **88**, 074002 (2013) [doi:10.1103/PhysRevD.88.074002](https://doi.org/10.1103/PhysRevD.88.074002) arXiv:1307.5683 [hep-ph].

[22] R. Aaij *et al.* [LHCb], Phys. Rev. Lett. **113**, 151601 (2014) [doi:10.1103/PhysRevLett.113.151601](https://doi.org/10.1103/PhysRevLett.113.151601) arXiv:1406.6482 [hep-ex].

[23] R. Aaij *et al.* [LHCb], JHEP **08**, 055 (2017) [doi:10.1007/JHEP08\(2017\)055](https://doi.org/10.1007/JHEP08(2017)055) arXiv:1705.05802 [hep-ex].

[24] C. Langenbruch [LHCb], arXiv:1805.04370 [hep-ex].

[25] A. López Huertas [LHCb], PoS **EPS-HEP2023**, 352 (2024) [doi:10.22323/1.449.0352](https://doi.org/10.22323/1.449.0352).

[26] A. Hayrapetyan *et al.* [CMS], Rept. Prog. Phys. **87**, 077802 (2024) [doi:10.1088/1361-6633/ad4e65](https://doi.org/10.1088/1361-6633/ad4e65) arXiv:2401.07090 [hep-ex].

[27] W. Altmannshofer and P. Stangl, Phys. Rev. D **105**, 035012 (2022) [doi:10.1103/PhysRevD.105.035012](https://doi.org/10.1103/PhysRevD.105.035012) arXiv:2103.13370 [hep-ph].

[28] M. Algueró, B. Capdevila, A. Crivellin, S. Descotes-Genon, P. Masjuan, J. Matias and J. Virto, Eur. Phys. J. C **79**, 714 (2019) [doi:10.1140/epjc/s10052-019-7216-3](https://doi.org/10.1140/epjc/s10052-019-7216-3) arXiv:1903.09578 [hep-ph].

[29] A. Khodjamirian, T. Mannel and Y. M. Wang, JHEP **02**, 010 (2013) [doi:10.1007/JHEP02\(2013\)010](https://doi.org/10.1007/JHEP02(2013)010) arXiv:1211.0234 [hep-ph].

[30] S. Li, Y. Xiao and J. M. Yang, *Mod. Phys. Lett. A* **36**, 2130022 (2021) [doi:10.1142/S0217732321300229](https://doi.org/10.1142/S0217732321300229) [arXiv:2110.04673 \[hep-ph\]](https://arxiv.org/abs/2110.04673).

[31] D. P. Aguillard *et al.* [Muon g-2], *Phys. Rev. Lett.* **131**, 161802 (2023) [doi:10.1103/PhysRevLett.131.161802](https://doi.org/10.1103/PhysRevLett.131.161802) [arXiv:2308.06230 \[hep-ex\]](https://arxiv.org/abs/2308.06230).

[32] A. Khodjamirian, T. Mannel, A. A. Pivovarov and Y. M. Wang, *JHEP* **09**, 089 (2010) [doi:10.1007/JHEP09\(2010\)089](https://doi.org/10.1007/JHEP09(2010)089) [arXiv:1006.4945 \[hep-ph\]](https://arxiv.org/abs/1006.4945).

[33] S. Jäger and J. Martin Camalich, *JHEP* **05**, 043 (2013) [doi:10.1007/JHEP05\(2013\)043](https://doi.org/10.1007/JHEP05(2013)043) [arXiv:1212.2263 \[hep-ph\]](https://arxiv.org/abs/1212.2263).

[34] J. Lyon and R. Zwicky, *Phys. Rev. D* **88**, 094004 (2013) [doi:10.1103/PhysRevD.88.094004](https://doi.org/10.1103/PhysRevD.88.094004) [arXiv:1406.0566 \[hep-ph\]](https://arxiv.org/abs/1406.0566).

[35] C. Bobeth, M. Chrzaszcz, D. van Dyk and J. Virto, *Eur. Phys. J. C* **78**, 451 (2018) [doi:10.1140/epjc/s10052-018-5918-6](https://doi.org/10.1140/epjc/s10052-018-5918-6) [arXiv:1707.07305 \[hep-ph\]](https://arxiv.org/abs/1707.07305).

[36] M. J. Aslam, C. D. Lü and Y. M. Wang, *Phys. Rev. D* **79**, 074007 (2009) [doi:10.1103/PhysRevD.79.074007](https://doi.org/10.1103/PhysRevD.79.074007) [arXiv:0902.0432 \[hep-ph\]](https://arxiv.org/abs/0902.0432).

[37] W. Wang, Y. M. Wang, D. S. Du and C. D. Lü, *Phys. Rev. D* **78**, 014006 (2008) [doi:10.1103/PhysRevD.78.014006](https://doi.org/10.1103/PhysRevD.78.014006) [arXiv:0804.2204 \[hep-ph\]](https://arxiv.org/abs/0804.2204).

[38] C. H. Chen and C. Q. Geng, *Phys. Rev. D* **71**, 115004 (2005) [doi:10.1103/PhysRevD.71.115004](https://doi.org/10.1103/PhysRevD.71.115004) [arXiv:hep-ph/0504145 \[hep-ph\]](https://arxiv.org/abs/hep-ph/0504145).

[39] W. Buchmüller, R. Rückl and D. Wyler, *Phys. Lett. B* **191**, 442–448 (1987) [Erratum: *Phys. Lett. B* **448**, 320 (1999)] [doi:10.1016/0370-2693\(87\)90637-X](https://doi.org/10.1016/0370-2693(87)90637-X).

[40] I. Doršner, S. Fajfer, A. Greljo, J. F. Kamenik and N. Košnik, *Phys. Rept.* **641**, 1–68 (2016) [doi:10.1016/j.physrep.2016.06.001](https://doi.org/10.1016/j.physrep.2016.06.001) [arXiv:1603.04993 \[hep-ph\]](https://arxiv.org/abs/1603.04993).

[41] J. M. Arnold, B. Fornal and M. B. Wise, *Phys. Rev. D* **88**, 035009 (2013) [doi:10.1103/PhysRevD.88.035009](https://doi.org/10.1103/PhysRevD.88.035009) [arXiv:1304.6119 \[hep-ph\]](https://arxiv.org/abs/1304.6119).

[42] S. Davidson, D. C. Bailey and B. A. Campbell, *Z. Phys. C* **61**, 613–644 (1994) [doi:10.1007/BF01552629](https://doi.org/10.1007/BF01552629) [arXiv:hep-ph/9309310 \[hep-ph\]](https://arxiv.org/abs/hep-ph/9309310).

[43] S. Fajfer, J. F. Kamenik and I. Nišandžić, *Phys. Rev. D* **85**, 094025 (2012) [doi:10.1103/PhysRevD.85.094025](https://doi.org/10.1103/PhysRevD.85.094025) [arXiv:1203.2654 \[hep-ph\]](https://arxiv.org/abs/1203.2654).

[44] B. Gripaios, M. Nardecchia and S. A. Renner, *JHEP* **05**, 006 (2015) [doi:10.1007/JHEP05\(2015\)006](https://doi.org/10.1007/JHEP05(2015)006) [arXiv:1412.1791 \[hep-ph\]](https://arxiv.org/abs/1412.1791).

[45] A. Crivellin, D. Müller and T. Ota, *JHEP* **09**, 040 (2017) [doi:10.1007/JHEP09\(2017\)040](https://doi.org/10.1007/JHEP09(2017)040) [arXiv:1703.09226 \[hep-ph\]](https://arxiv.org/abs/1703.09226).

[46] T. M. Aliev, K. Azizi and M. Savci, *Phys. Rev. D* **76**, 074017 (2007) [doi:10.1103/PhysRevD.76.074017](https://doi.org/10.1103/PhysRevD.76.074017) [arXiv:0710.1508 \[hep-ph\]](https://arxiv.org/abs/0710.1508).

[47] E. Kou *et al.* [Belle II], *PTEP* **2019**, 123C01 (2019) [doi:10.1093/ptep/ptz106](https://doi.org/10.1093/ptep/ptz106) [arXiv:1808.10567 \[hep-ex\]](https://arxiv.org/abs/1808.10567).

[48] F. Abudinén *et al.* [Belle II], [arXiv:2110.08219 \[hep-ex\]](https://arxiv.org/abs/2110.08219).

[49] R. Aaij *et al.* [LHCb], LHCb-PUB-2018-009 (Upgrade II physics case) [arXiv:1808.08865 \[hep-ex\]](https://arxiv.org/abs/1808.08865).

[50] I. Bediaga *et al.* [LHCb], “Physics case for an LHCb Upgrade II,” CERN-LHCC-2018-027, LHCb-PUB-2018-009 [arXiv:1808.08865 \[hep-ex\]](https://arxiv.org/abs/1808.08865).

[51] S. de Boer, B. Müller and D. Seidel, *JHEP* **08**, 091 (2016) [doi:10.1007/JHEP08\(2016\)091](https://doi.org/10.1007/JHEP08(2016)091) [arXiv:1606.05521 \[hep-ph\]](https://arxiv.org/abs/1606.05521).

[52] R. N. Faustov and V. O. Galkin, *Eur. Phys. J. C* **78**, 527 (2018) [doi:10.1140/epjc/s10052-018-6010-y](https://doi.org/10.1140/epjc/s10052-018-6010-y) [arXiv:1805.02516 \[hep-ph\]](https://arxiv.org/abs/1805.02516).

[53] K. Azizi, A. T. Olgun and Z. Tavukoglu, *Adv. High Energy Phys.* **2017**, 7435876 (2017) [doi:10.1155/2017/7435876](https://doi.org/10.1155/2017/7435876) [arXiv:1609.09678 \[hep-ph\]](https://arxiv.org/abs/1609.09678).

[54] C. H. Chen, C. Q. Geng, C. C. Lih and C. C. Liu, “Study of $B \rightarrow K_0^*(1430) \ell \bar{\ell}$ decays,” *Phys. Rev. D* **75**, 074010 (2007), [doi:10.1103/PhysRevD.75.074010](https://doi.org/10.1103/PhysRevD.75.074010) [arXiv:hep-ph/0703106 \[hep-ph\]](https://arxiv.org/abs/hep-ph/0703106).